

A Numerical Model to Study the Interaction of Vascular Stents with Human Atherosclerotic Lesions

DIMITRIOS E. KIOUSIS,¹ T. CHRISTIAN GASSER,¹ and GERHARD A. HOLZAPFEL^{1,2}

¹Department of Solid Mechanics, School of Engineering Sciences, Royal Institute of Technology (KTH), Stockholm, Sweden; and ²Institute for Biomechanics, Center for Biomedical Engineering, Graz University of Technology, Kronesgasse 5-I, 8010 Graz, Austria

(Received 9 February 2007; accepted 10 July 2007; published online 24 July 2007)

Abstract—A methodology is proposed that identifies optimal stent devices for specific clinical criteria. It enables to predict the effect of stent designs on the mechanical environment of stenotic arteries. In particular, we present a numerical study which is based on the interaction of a vascular stent with a patient-specific, atherosclerotic human iliac lesion of type V. The stress evolution in four different tissue components during and after stenting is investigated. The geometric model of the artery is obtained through MRI, while anisotropic material models are applied to describe the behavior of tissues at finite strains. In order to model the observed fissuring and dissection of the plaque under dilation, the undeformed configuration of the arterial wall incorporates two initial tears. The 3D balloon-stent-artery interaction problem is modeled by means of a contact algorithm, which is based on a C^2 -continuous surface parametrization, hence avoiding numerical instabilities of standard facet-based techniques. In the simulations three different stent designs are studied. The performance of each stent is characterized by scalar quantities relating to stress changes in the artery, contact forces, and changes in lumen area after stenting. The study concludes by suggesting two optimal stent designs for two different clinically relevant parameters.

Keywords—Atherosclerosis, Balloon angioplasty, Contact, Finite element method, Mechanical stress, Modeling, MRI, Stent.

INTRODUCTION

Balloon angioplasty with stenting is a well established and effective vascular reconstructive procedure aiming to reduce the severity of atherosclerotic stenosis, one of the most frequent form of cardiovascular diseases. Its popularity arises due to its less invasive nature (compared to surgical alternatives) and better

clinical outcome (compared to balloon angioplasty without stenting^{9,36}).

Despite the constantly increasing success rate of stenting through technological progresses in stent design and drug coatings on the stents' surface,⁴ the procedure can still fail because of in-stent restenosis which occurs in 30–60% of patients with complex lesions.⁶ Restenosis is a mechanobiological process characterized by stress-induced growth, such as neo-intimal hyperplasia. In more detail, the focal vascular trauma imposed by the struts of the stent, the stress and strain environments around the expanded stent, and the existence of a foreign material in the injured artery may trigger molecular mechanisms, leading to inflammation, granulation, and extracellular matrix production.^{35,42,44} These processes may lead to reclosure of the blood vessel, which results in the need for further interventions.

Balloon angioplasty with stenting is a procedure of mainly mechanical characteristics. It is, therefore, understandable that its outcome depends on the design parameters defining the mechanics of the stent such as the material and the geometry of stent cells and struts. This is supported by recent clinical studies,^{21,31} which identified the stents' geometric characteristics as one of the major elements for reducing or increasing the risk of restenosis. Toward this direction, numerical tools such as the finite element method have been recently applied in order to investigate the biomechanical implications of vascular stenting and to provide optimal configurations of medical devices.

A literature survey on the recently published numerical attempts to model atherosclerotic lesions revealed that, still in the majority of computational models developed in recent years, the non-diseased arterial wall and the plaque are frequently modeled as a homogeneous and single-layer structure.^{3,25,30} In addition, several models assume the arterial tissue to be isotropic, which do not reflect the experimentally

Address correspondence to Gerhard A. Holzapfel, Institute for Biomechanics, Center for Biomedical Engineering, Graz University of Technology, Kronesgasse 5-I, 8010 Graz, Austria. Electronic mail: holzapfel@tugraz.at

observed cylindrically orthotropic behavior of non-diseased^{1,11,14,33,34,43,48} and diseased^{13,15} vascular tissues. It seems also that only a few studies have considered three-dimensional (3D) geometries.^{16,17,22} Although simplified approaches have contributed to the current level of understanding of angioplasty mechanics, there is a need to model the actual 3D morphology and the related mechanics in a more realistic way and on a patient-specific basis. To the best of the authors' knowledge, the study by Liang *et al.*²⁸ was the first to incorporate the balloon in a simulation considering a stent, however, simplified, cylindrical geometries were considered. A detailed approach seems to be the one documented by Holzapfel *et al.*,¹⁶ where the accounted arterial geometry consisted of eight different tissue models, obtained through high-resolution magnetic resonance imaging (hrMRI), while anisotropic material models were applied to describe the behavior of tissues at finite strains. As in the previously mentioned attempts, the contact interaction of the balloon catheter was not modeled. In addition, the used finite element meshes and the geometric representation of the arterial wall were not particularly fine.

The present work is a step towards improving the numerical modeling of balloon angioplasty with stenting by taking the interaction of vascular stents with human atherosclerotic lesions into account. Three-dimensional morphological data of a type V atherosclerotic lesion³⁷ of an iliac artery are considered. The arterial wall is modeled as a non-homogeneous solid, consisting of four different tissue components. The applied constitutive models are able to capture the nonlinear, anisotropic behavior of arterial tissues. A vascular stent, received from a stent-producing company, is parameterized. In addition, two modified geometric designs are generated. A cylindrically orthotropic model is used in order to describe the anisotropic behavior of balloon catheters under internal pressure load. Balloon angioplasty with stenting is numerically performed by solving the balloon-stent-artery interaction as a 3D contact problem. For this purpose, a C^2 -continuous surface description is applied, which prevents numerical instabilities arising from non-smooth body discretization.^{22,38} The proposed computational model also attempts to provide a deeper insight into the dominating effect of plaque fissuring and dissection during stenting.^{5,27,29} This is performed by introducing two (small) initial cracks near the edges of the plaque.

The study results in the identification of changes in the mechanical environment of the artery during and after stenting, when the three different stent designs are used. Particular emphasis is placed on the generated stress fields of the four arterial tissues. The performance of the different stents is quantified by means of

three scalar indicators.¹⁶ These indicators characterize the lumen gain and the arterial injury imposed by the stents. Therefore, they may be helpful in finding the optimal stent design for the particular stenosis and for specific optimization criteria.

The manuscript is organized as follows: we start by providing details on the geometric and material modeling of the arterial wall, the balloon, and the considered stents. We place particular emphasis on the finite element model of the 3D problem of stenting. The contact of the involved bodies, the discretization, the loading procedure, and the three indicators of the stent-artery interaction are described. Next, we demonstrate the most important findings of the performed numerical simulations and compare the outcome of the stenting procedure for the different stent designs. Finally, we summarize the presented numerical model and discuss its features and limitations.

GEOMETRIC AND MATERIAL MODELING

This section provides the geometric and material modeling aspects of the vessel wall and the involved medical devices, i.e., the balloon catheter and the stent. The section starts by the description of the 3D arterial model based on image data, and introduces the adopted continuum formulation, which is able to incorporate the nonlinearity and anisotropy inherent in human tissues. Next, account of a stent model, based on a currently used product, is given and finally a cylindrically orthotropic material model is presented in order to describe the deformation of angioplasty balloons under internal pressure.

Arterial Model

In the present numerical study, a detailed geometric and physical model of an atherosclerotic-prone human external iliac artery (65 years, female) is considered. The regarded lesion is of type V, according to the classification proposed by Stary.³⁷ This type of stenosis is characterized by prominent new fibrous connective tissue and a lipid core. The 3D geometry of the arterial wall architecture was traced by means of hrMRI and reconstructed by non-uniform rational B-splines (NURBS), as can be seen in Fig. 1(I). A detailed description of the procedure and the associated histological analyses, required to identify the underlying tissue types, is provided in Auer *et al.*² and Holzapfel *et al.*¹⁵ The identification of the 3D tissue structure is regarded as an important aspect of the documented attempt, and it is a necessary prerequisite of meaningful simulations of balloon angioplasty with stenting. According to the classification proposed by Holzapfel

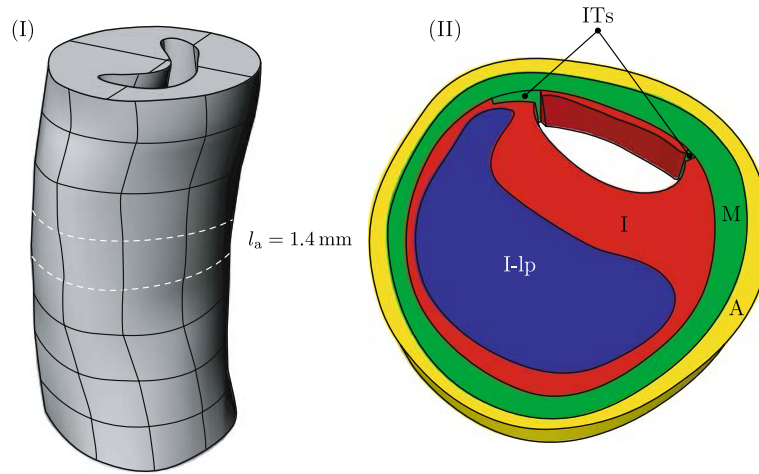


FIGURE 1. (I) 3D geometric model of a stenotic human iliac artery obtained from hrMRI and reconstructed by means of NURBS. (II) Extracted arterial slice with length $l_a = 1.4$ mm, composed by four arterial tissues: adventitia (A), media (M), intima (I), and lipid pool (I-lp). The introduced initial tears (ITs) are also indicated.

et al.,¹⁵ seven different tissue types are identified in the atherosclerotic arterial wall: adventitia (A), non-diseased media (M-nos), non-diseased intima (I-nos), fibrous cap (I-fc), fibrous intima at the medial border (I-fm), lipid pool (I-lp), and fibrous media (M-f). For the purpose of this study, M-nos and M-f are combined to one tissue component referred to as ‘media’ (M), and I-nos, I-fc, and I-fm are combined to another component referred to as ‘intima’ (I). The consideration of all seven arterial tissues would require detailed information about the anisotropy of each individual tissue, as discussed later in this section. From the complete arterial wall a section with length $l_a = 1.4$ mm (which is also the smallest cell length of the stent) is considered, which incorporates four tissue types (see Fig. 1).

Balloon angioplasty and stenting frequently lead to fissuring and dissection of the atherosclerotic plaque,⁵ which is thought to be one of the main mechanisms of lumen gain obtained through this procedure. A reliable prediction of the stress field of the stented arterial wall requires the incorporation of these effects. However, the present work does not investigate the fissuring and dissection from a fracture mechanics point of view, as performed recently by, for example, Gasser and Holzapfel.⁸ Instead two initial tears (ITs) are introduced into the intima. A similar approach is published by Gasser and Holzapfel.⁷ The initial cracks are placed at the edges of the plaque (the plaque shoulder) because experimental studies indicate these locations as the most prominent ones to plaque rupture.^{27,29} The arterial slice described above is depicted in Fig. 1(II).

The choice of the constitutive response used for the involved tissue components is of fundamental importance for the reliable prediction of the evolution of stresses and strains during stenting. For the determination of the passive, quasi-static mechanical

properties of the individual tissue components, mechanical tests were performed on a computer-controlled, screw-driven, high-precision tensile machine. Rectangular stripe samples with axial and circumferential orientations were excised and stretched far beyond their physiological loading domain in order to capture the range of deformations induced by the stent. The lipid pool did not allow tensile testing due to its fluid-like consistency. A detailed description of the performed mechanical tests is documented in the study.¹³

Arterial tissues are anisotropic, heterogeneous, highly deformable, (nearly) incompressible and show a pseudo-elastic behavior.¹⁸ Following the work,¹² it is assumed that each tissue component is reinforced by two families of collagen fibers embedded in an isotropic ground matrix. This reinforcement renders the material properties anisotropic. The fibers’ (mean) preferred directions are represented by two unit vectors, say \mathbf{a}_{01} and \mathbf{a}_{02} . The isochoric part $\bar{\Psi}$ of the strain-energy stored in the non-collageneous and collageneous components is given by¹²

$$\bar{\Psi} = \bar{\Psi}(\bar{I}_1, \bar{I}_4, \bar{I}_6) = \mu(\bar{I}_1 - 3) + \frac{k_1}{2k_2} \sum_{i=4,6} \left\{ \exp \left[k_2(\bar{I}_i - 1)^2 \right] - 1 \right\}, \quad (1)$$

where $\bar{I}_1 = \text{tr} \bar{\mathbf{C}}$ is the first invariant of the modified Cauchy–Green tensor $\bar{\mathbf{C}} = J^{-2/3} \mathbf{C}$,¹⁰ and $\bar{I}_4 = \bar{\mathbf{C}} : \mathbf{a}_{01} \otimes \mathbf{a}_{01}$ and $\bar{I}_6 = \bar{\mathbf{C}} : \mathbf{a}_{02} \otimes \mathbf{a}_{02}$ are two invariants. The material parameters μ and k_1 have dimensions of stress, while k_2 is a dimensionless parameter. The first part of Eq. (1) models the contribution of the non-collageneous ground matrix, while the second part, characterizes the energy stored in the collagen fibers.

The strain-energy described in Eq. (1) is used for each of the four tissue components, but with a different set (μ , k_1 , k_2) of material parameters, and different direction vectors (\mathbf{a}_{01} and \mathbf{a}_{02}) associated with the structure. Up to now, there are unfortunately no data available in the literature, concerning the collagen structure of stenotic iliac arteries. In the present approach, the structural data \mathbf{a}_{01} and \mathbf{a}_{02} are treated phenomenologically and are estimated from the mechanical tests described previously. In addition, the components of the collagen fibers' direction vectors in the radial direction are neglected, allowing thus the description of \mathbf{a}_{01} and \mathbf{a}_{02} by an angle α , defined between the fiber reinforcement and the circumferential direction of the individual layer. The least-square fitting of the constitutive model to the anisotropic data reported in Holzapfel *et al.*¹⁷ leads to the determination of the three involved material parameters (μ , k_1 , k_2) and the structural parameter α . The obtained values are summarized in Table 1.

Stent Models

First we considered an EXPRESS VASCULAR LDTM stent with delivery system (guide wire and introducer sheath) obtained from BOSTON SCIENTIFIC SVERIGE AB. The detailed shape and dimensions of the undeformed configuration of the stent, shown in Fig. 2(I), were studied using an Olympus reflected-light microscope with an attached digital camera.

The 3D computer model of the stent (Fig. 2(II)) is generated by means of a parametrization algorithm. Parametric design is a useful technique in engineering when products are tailored fit to specific needs or when optimization is used to generate the optimal product design. In the present work, the developed program, aids to the fast generation of different configurations of the provided stent. The algorithm makes use of a series of design parameters, describing the stent's morphology and dimensions. These parameters are depicted in Fig. 2(II). In addition, the parametrization algorithm is able to provide the finite element mesh of the individual parameterized stent.

TABLE 1. Material and structural parameters of different tissue types, describing the anisotropic response of an atherosclerotic iliac lesion of type V.

Tissue	μ (kPa)	k_1 (kPa)	k_2 (-)	α (°)
Adventitia (A)	1.75	65.6	61.8	± 49.0
Media (M)	15.0	4.0	2.3	± 7.0
Intima (I)	78.9	23.7	26.3	0.0
Lipid pool (I-lp)	0.1	0.0	-	-

Data taken from Holzapfel *et al.*¹⁷

In the simulations described below, three stent designs are taken into consideration. The first is the obtained stent from BOSTON SCIENTIFIC SVERIGE AB (control stent, labeled as S_1 , with specific dimensions shown in Fig. 2(III)), while the two other designs derive from variations of the parameters defining the width of the struts (s_i) and the wave length of the stent's cell (l_{st}), see Table 2. The first variation of the control stent, labeled as S_2 , has thinner struts (more compliant structure), while the second variation labeled as S_3 , has approximately half of the struts of the control stent (stiffer structure). Since only a slice of the vessel wall is studied, only one cell of the stent is considered.

According to the acquired data, the EXPRESS VASCULAR LDTM stent is made of stainless steel (316L). The material's elastic regime is described by a neo-Hookean model, while its inelastic response is described by a von Mises–Hill plasticity model with linear hardening. The Young's modulus is $E = 201$ GPa and the Poisson's ratio is $\nu = 0.3$. The yield stress σ_y is chosen equal to 300 MPa and the hardening modulus H_{iso} is equal to 2 GPa.

Balloon Catheter Model

Although the initial form of balloon catheters is S- or Z-shaped, the undeformed configuration of the balloon is modeled as a circular cylinder. The outer diameter of the cylindrical balloon is $D_{b,o} = 2.2$ mm, the thickness $H_b = 0.2$ mm and the length $l_b = 2.0$ mm.

The inflation of balloon catheters is characterized by complex kinematics. Initially, the unfolding of the balloon takes place under low internal pressure. Further increase of the pressure, leads to a continuously increasing diameter, while the catheter retains axially its cylindrical shape. After a specific load, depending on the balloon's mechanical and geometric properties, the balloon exposes rapidly a nonlinear, stiffening behavior. In order to account for the described effects, a cylindrically orthotropic model, based on fiber-reinforced materials' theory, was developed.²² Briefly, two material axes with different mechanical properties are introduced, oriented in the axial and circumferential directions. Circumferentially, the balloon is very soft initially but particularly stiff after a predefined stretch limit, provided by the stent manufacturer. In the longitudinal direction the balloon is assumed to be already stiff at its reference direction, hence the axial stretch limit is about 1. The introduction of this artificial material allows the imitation of the typical characteristics of balloon catheters.²² Note that this peculiar mechanical response could not be obtained by means of isotropic material models.

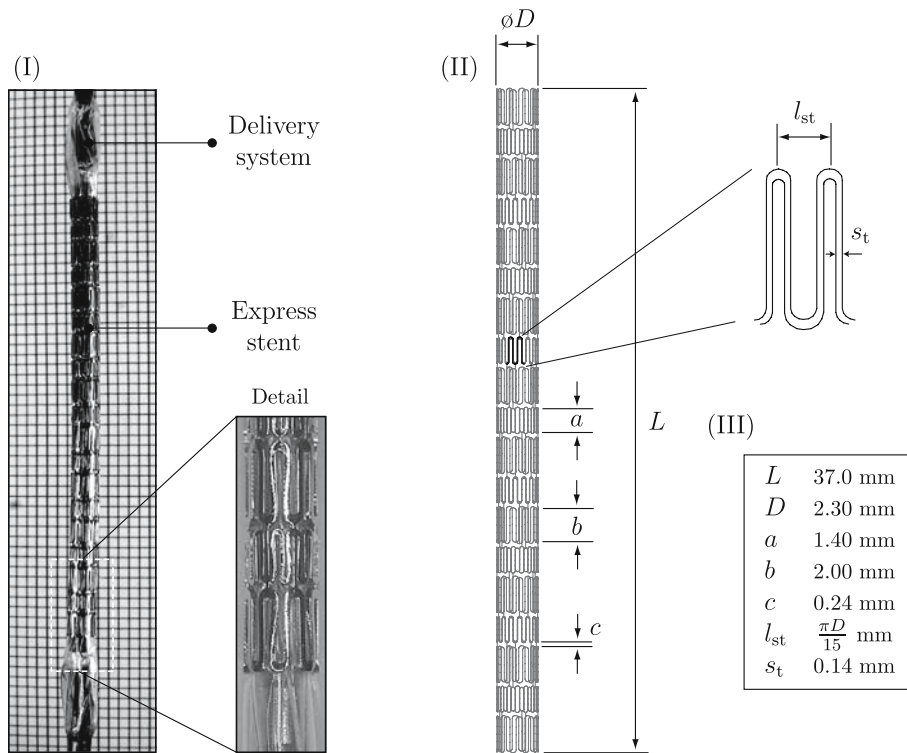


FIGURE 2. (I) Photograph of the undeformed configuration of the pre-mounted EXPRESS VASCULAR LD™ stent and detailed view of the stent's sinusoidal-structured cells. (II) 3D geometric model of the stent, obtained by a parametrization algorithm that makes use of the shown design parameters. (III) Dimensions of the obtained stent.

TABLE 2. Values of the geometric parameters of the three different stent designs used in the simulations of balloon angioplasty with stenting.

Stent configurations	s_t (mm)	l_{st} (mm)
S_1 (control stent)	0.14	$\pi D/15$
S_2 (thinner struts)	0.10	$\pi D/15$
S_3 (fewer struts)	0.14	$\pi D/7$

The value of the diameter D is given in Fig. 2.

NUMERICAL SIMULATIONS

This section summarizes the developed finite element model of balloon angioplasty with stenting, including the modeling of the contact interactions between the balloon, the stent, and the arterial wall. The generation of the computational grid is thoroughly described, and the chosen boundary conditions along with the loading procedure are given. Finally, three indicators able to characterize the stent–artery interaction are discussed in detail.

Contact Modeling

For the finite element simulation of contact problems concerning finite deformation, large sliding and arbitrarily curved contact surfaces, standard facet-based contact algorithms may lead to numerical prob-

lems. In particular, oscillation of contact forces, non-realistic pressure jumps and finally loss of quadratic convergence are observed, which arise from the sliding of nodes over facets' boundaries, where jumps of the normal vector are experienced.⁴⁷ Therefore, the 3D numerical modeling of contact interactions during balloon angioplasty with stenting requires an advanced and robust contact approach. To address the problem mentioned above, and to successfully simulate the contact interactions between the medical devices and the arterial wall, the algorithm based on C^2 -continuous uniform cubic B-spline surfaces documented in Kioussis *et al.*²² and implemented into the multipurpose finite element analysis program FEAP,⁴⁰ is adopted.

In more detail, the involved contact pairs in the simulation are: (i) stent–balloon; (ii) stent–artery; and (iii) balloon–artery. The first body in all pairs is considered as the contractor (slave) body, while the second as the target (master) body. Following the node-to-surface contact approach, the surfaces of the contractors are described by their superficial finite element nodes \mathbf{x}^s . The target surfaces are described by cubic B-spline surfaces \mathbf{S}^m .

A uniform cubic B-spline is obtained by taking a bidirectional mesh of 4×4 control points $\mathbf{P}_{i,j}$, $i, j = 1, \dots, 4$, and the products of the univariate cubic basis functions³²

$$\left. \begin{aligned} B_1(t) &= (1 - 3t + 3t^2 - t^3)/6, \\ B_2(t) &= (4 - 6t^2 + 3t^3)/6, \\ B_3(t) &= (1 + 3t + 3t^2 - 3t^3)/6, \\ B_4(t) &= t^3/6. \end{aligned} \right\} \quad (2)$$

Thus, the mathematical representation of the uniform cubic B-spline surfaces is

$$\mathbf{S}(u, v) = \sum_{i=1}^4 \sum_{j=1}^4 B_i(u)B_j(v)\mathbf{P}_{ij}, \quad 0 \leq u, v \leq 1, \quad (3)$$

where u and v are convective coordinates, and the parameter t in Eq. (2) stands for either u or v . For illustrative reasons, Fig. 3 is given to show the geometrical situation. In Fig. 3(I) an example of a 4×4 control mesh and its corresponding uniform cubic B-spline surfaces is shown (plotted in MATHEMATICA⁴⁵). In Fig. 3(II) two overlapping control polyhedrons and two adjacent uniform cubic B-spline surfaces (\mathbf{S}_1 and \mathbf{S}_2) are illustrated. The C^2 -continuous border between the two surfaces is also indicated.

In the presented method, the required structured meshes of control points (noted above as \mathbf{P}_{ij}) for the parametrization of the contact surfaces are generated by the finite element nodes located on the target surfaces. This approach yields a robust interface between the smooth surface and the continuum body. Following the penalty method as the regularization technique for the inequality variational principle of the contact conditions,^{26,46} a gap function g_N is defined for each contact pair as

$$g_N = (\mathbf{x}^s - \mathbf{x}^{m*}) \cdot \mathbf{n}^{m*}, \quad (4)$$

where \mathbf{x}^{m*} is the orthogonal projection of the contractor node \mathbf{x}^s on the target surface \mathbf{S}^m , and \mathbf{n}^{m*} is the outward unit normal vector at \mathbf{x}^{m*} . Here \mathbf{x}^{m*} is the solution of a minimum distance problem, which leads

to a local Newton iteration for the present problem. From Fig. 3(II) it is obvious that as a contractor node slides over the boundaries of the B-spline target surfaces (e.g., from \mathbf{S}_1 to \mathbf{S}_2), the normal vector \mathbf{n}^{m*} changes smoothly. This is not the case, when first-order facets are used to represent the target surfaces.

The gap function g_N defines the state of contact, and together with the penalty stiffness it quantifies the contact contribution $\delta W_{\text{ext},c}$ to the external virtual work, which is given by

$$\delta W_{\text{ext},c} = \int_{\Gamma_c^s} t_N \delta g_N d\Gamma_c^s, \quad (5)$$

where t_N is the normal contact force and Γ_c^s the contact surface boundary. The residual vector and the stiffness matrix for the finite element implementation of the model are computed by applying the MATHEMATICA package ACEGEN.²⁴ To this end, several novel techniques such as automatic differentiation and stochastic evaluation of formulas are used. For a detailed description of the developed contact algorithm, the reader is referred to the work by Kiousis *et al.*²²

It is worth mentioning, that the employed formulation allows the incorporation of frictional contact. Nevertheless, the simulations are carried out without friction since reliable coefficients describing the frictional behavior between the intimal surface, the balloon catheter, and the stent are not yet available.

Finite Element Discretizations

The 3D geometric models of the four arterial tissues are separately discretized by application of the commercial mesh generation toolkit CUBIT.⁴¹ Approximately 3500 eight-node hexahedral elements are generated in total, and the mixed finite element formulation, as implemented in FEAP, is applied. This

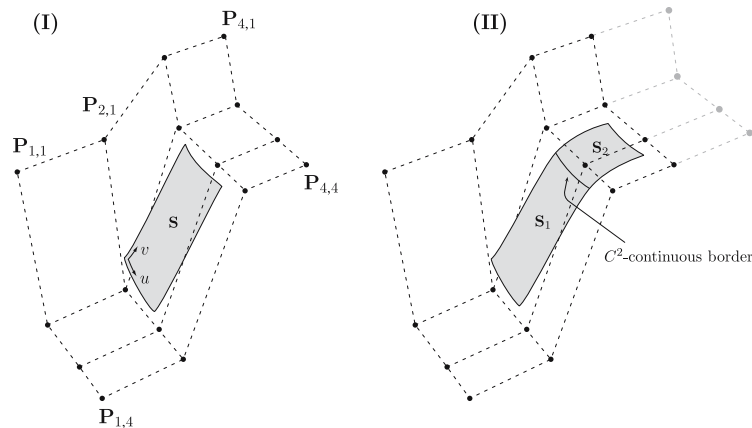


FIGURE 3. (I) A 4×4 mesh with control points $\mathbf{P}_{ij}, i, j = 1, \dots, 4$, and its corresponding uniform cubic B-spline surface. (II) Two overlapping control meshes and two adjacent B-spline surfaces with C^2 -continuous borders.

approach provides an efficient and proper description of the incompressible deformation of arterial tissues. The meshes are generated with matching nodes on the tissue interfaces, and hence no special algorithmic treatment is required to link them. The generated mesh of the intima also satisfies the requirement of the discussed contact algorithm, i.e., structured quadrilateral facets on the contact surface. The same type of volume elements is chosen for the discretization of the balloon catheter, where 288 elements are generated. Finally, the structure of the stent implies the use of two-node, large displacement, large rotation 3D frame elements.¹⁹ The choice of frame elements over hexahedral elements also leads to less computationally expensive simulations, an important aspect when complex contact problems are to be analyzed.

Boundary Conditions

Experience obtained through experimental investigations showed that, in contrast to healthy arteries, highly stenotic human vessels show very little or no axial *in situ* pre-stretch, approximately equal to 1 (a value of 1.03 is reported in Holzapfel *et al.*¹³). Hence, no axial forces or displacements are applied to the artery. The top and bottom faces of the considered artery section are fixed in the axial direction (plane strain condition). The load-free configuration of the arterial wall (shown in Fig. 1(II)) is also considered stress free, and hence residual strains (stresses) are neglected. Even though the algorithmic concept for the incorporation of residual stresses exists,³⁹ the lack of experimental data in atherosclerotic lesions makes their consideration not possible in this work. Next, a small value of stiffness is given to each node of the artery. This restricts the rigid motion of the artery. To obtain an almost concentric expansion of the balloon catheter, its nodes located on two orthogonal axial planes are bounded in the circumferential direction. As far as the stent is concerned, the axial displacements are fixed for all the nodes on its midplane, thus, restricting its rigid motion.

Loading Procedure

The reference diameter of the chosen catheter and stent is bigger than the diameter of the lumen of the stenotic vessel under investigation. Hence, the undeformed balloon and stent are placed in the lumen with penetration. Next, the penalty parameter which enforces the contact constraint is gradually increased in a few load steps. Thus, the penetration is reduced and the contact between the medical devices and the inner arterial wall is established in a numerically stable way. The expansion of the balloon catheter follows. This is

performed by follower pressure loads which are applied on the inner surface of the balloon. As the balloon expands, it comes into contact with the stent and the artery. Further increase of the inner balloon pressure leads to the expansion of the three bodies. When the outer diameter of the balloon reaches a desired value, the balloon contact penalty parameter is gradually decreased, simulating the balloon catheter's deflation, and only the plastically deformed stent remains in contact with the inner surface of the vessel.

Indicators for the Outcome of Angioplasty

Local stress distributions within the specimen during balloon angioplasty and stenting are undoubtedly an important measure to illustrate the changes in the mechanical environment of the vessel wall caused by a particular stent. Nevertheless, if criteria are based on a set of scalar quantities and linked to mechanical measures such as contact forces and stresses, then they could provide a faster and more comprehensive and reliable judgment of the stent–stenosis interaction. The idea to introduce scalar indicators, characterizing the mechanical field of the arterial wall and the lumen change after stenting, was initially proposed in Holzapfel *et al.*,¹⁶ while also applied in Bedoya *et al.*³ and Kioussis *et al.*²² In order to compare the three different stent designs, the same approach is adopted here.

The first introduced indicator characterizes the contact force applied on the intimal surface from the stent's struts. This is an important measure, since elevated contact pressure in the vicinity of the stent struts may lead to injury of the endothelial and medial smooth muscle cells, which may increase the neointimal hyperplasia formation.²³ The indicator of the normalized contact forces at the intimal surface caused by the stent struts is denoted by D_1 , and expressed as

$$D_1 = \sum_{i=1}^{n_s} \frac{F_{i,\text{post}}}{l_c}, \quad (6)$$

where n_s is the total number of nodes of the stent cell and $F_{i,\text{post}}$ is the norm of the contact force at each stent node after stenting, given by

$$F_{i,\text{post}} = \left(\sum_{j=1}^3 f_j^2 \right)^{1/2}, \quad (7)$$

where f_j are the reaction force components at the node i , and l_c is the total length of the considered stent cell. The indicator D_1 can also be used as a measure for prolapse, hence as a measure for the deflection of tissue between the struts. Prolapse, depends strongly on the artery's (material) composition, the contact forces and the spacing between the stent

struts, thus it can be linked to D_1 . In addition, pro-lapse provides an important insight on the effectiveness of stenting since clinical studies relate it with the appearance of restenosis.²⁰

As aforementioned, a critical factor that drives restenosis is the long-term change of stresses within the arterial wall after the performance of the interventional treatment. High stresses induced by the stent may be responsible for the triggering of growth mechanisms and finally may lead to restenosis.⁴⁴ Therefore, a second indicator D_2 is used, able to quantify stress changes in the arterial wall. This indicator is defined as¹⁶

$$D_2 = \frac{\sum_{i=1}^{n_v} \Delta\sigma_i \Omega_i}{\sum_{i=1}^{n_v} \sigma_{i,MAP} \Omega_i}, \quad \Delta\sigma_i = \sigma_{i,post} - \sigma_{i,MAP}. \quad (8)$$

In the above equation, n_v denotes the number of the arterial volume elements and Ω_i the volume of the element i , which is used as a weighting factor. Next, $\sigma_{i,post}$ and $\sigma_{i,MAP}$ are the maximum (principal Cauchy) stress in the element i after stenting and under mean arterial pressure, respectively.

The last indicator, denoted by LG (Lumen Gain), corresponds to the lumen change due to stenting. The lumen gain LG is defined as¹⁶

$$LG = \frac{A_{post}}{A_{MAP}} - 1, \quad (9)$$

where A_{MAP} is the smallest inner cross-section of the artery before angioplasty and stenting, and A_{post} is the cross-section at the same location as A_{MAP} after angioplasty and stenting.

RESULTS

In the following section, the most illustrious results of the performed numerical simulations are provided. In particular, the stenting-induced stress fields of the arterial tissues are studied and the performance of the considered stent designs is analyzed using scalar indicators.

Predicted Stress Fields

The first of the performed simulations concerns the atherosclerotic lesion under internal pressure load. The

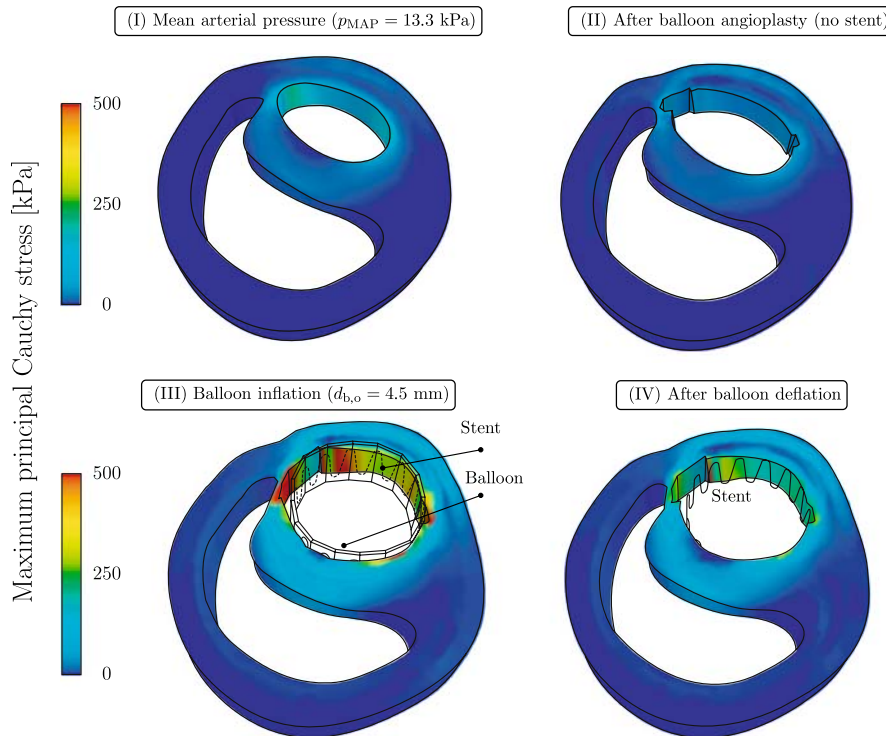


FIGURE 4. Deformed configuration and distribution of the maximum (principal Cauchy) stresses in the arterial tissues (intima, media, adventitia) of an atherosclerotic human iliac artery at different load states: (I) mean arterial pressure ($p_{MAP} = 13.3$ kPa), no initial tears present; (II) balloon angioplasty without stenting; (III) balloon and stent inflation (up to $d_{b,o} = 4.5$ mm); and (IV) after deflation of the balloon catheter (only the stent remains in contact with the arterial wall). The lipid pool is not shown.

chosen load is the mean arterial pressure, i.e., taken to be $p_{\text{MAP}} = 13.3$ kPa. Note that in this case no initial tears are incorporated since tissue dissection and fissuring are considered to take place at loadings which occur during balloon angioplasty. The stress field in this case is illustrated in Fig. 4(I). The maximum (principal Cauchy) stresses are given in kPa and are shown for the intima, media, and adventitia. As can be seen in Fig. 4(I), the innermost layer of the lesion is the main load carrier of the structure. This is analogous to inflated thick-wall tubes, where the stress concentration is located at the inner part of the wall. The deformed state, as shown in Fig. 4(I), is regarded as the pre-stenting reference state, indicated by $(\bullet)_{\text{MAP}}$.

Next, the (small) initial cracks at the intima are considered and the deformed configuration and stress distribution in the arterial tissues under the same loading conditions are studied (Fig. 4(II)). As previously mentioned, the role of the tears is to incorporate fissuring and dissection of the arterial tissues, which occur during angioplasty interventions.^{5,27,29} The above simulation aims to model the procedure of balloon angioplasty without stenting. The evolution of the crack tips due to the internal pressure is visible in Fig. 4(II).

The following step is concerned with the numerical modeling of stenting with reference to the undeformed configuration of the stenotic lesion including the two initial tears. The three different stent designs, as introduced within the section ‘Stent Models,’ are used for this purpose. Figures 4(III) and 4(IV) show the deformed shapes and the resulting stress fields at full balloon inflation and after deflation of the balloon catheter, respectively. Thereby the model of the ‘original’ (control) EXPRESS VASCULAR LDTM stent is used. In all cases the balloon is inflated until its outer diameter reaches the value $d_{b,o} = 4.5$ mm, which corresponds to an approximate balloon internal pressure of $p_b = 8$ bar. Then, the balloon is removed and only the stent remains in contact with the arterial wall. The slightly smaller lumen area, as shown in Fig. 4(IV), with respect to Fig. 4(III), reveals the recoil of the elastoplastic stent. As can be seen in the Figs. 4(II–IV), the tear of the intima and its dissection from the media, lead to a different stress field (when compared to the condition depicted in Fig. 4(I)). In the case of balloon angioplasty without and with stenting, the intact intima continues to carry the main part of the load, but the stresses in the adventitia and media increase during and after stenting (especially behind and at the tips of the dissections). In particular, a value of approximately 500 kPa is obtained at both tips at full balloon inflation (Fig. 4(III)). According to Holzapfel et al.,¹⁵ human atherosclerotic plaques of iliac arteries rupture at a stress level

similar to that computed here, which additionally justifies the incorporation of the (small) initial cracks. It is interesting to observe that in the diseased part of the intima a stress-shield in form of an arc is present. The acquired results also point out that the lipid pool is under a low compressive hydrostatic pressure. The obtained deformed shapes and stress fields, as illustrated in Fig. 4(IV), qualitatively and quantitatively agree with the outcome of a recent study,⁸ where plaque fissuring and dissection during angioplasty were modeled by means of a fracture propagation algorithm based on cohesive zones. However, therein, no stent is used and the analysis does not address contact interactions. Note that for all considered cases the highest stresses were obtained at the introduced crack tip.

Comparison of Different Stent Designs

At the end of the performed simulations of balloon angioplasty without and with stenting using the three stent designs, the aforementioned indicators D_1 , D_2 , LG are computed for each case. The obtained values are then normalized (from 0 to 1) according to

$$\overline{\text{ind}} = \frac{\text{ind} - \text{ind}_{\min}}{\text{ind}_{\max} - \text{ind}_{\min}}, \quad (10)$$

where ‘ind’ stands for the indicator D_1 , D_2 , and LG .

The quantities ind_{\max} and ind_{\min} refer to the maximum and minimum values of the related indicator with respect to the four cases, i.e., ‘balloon angioplasty (no stent),’ ‘control stent S_1 ,’ ‘stent with thinner struts S_2 ,’ and ‘stent with fewer struts S_3 .’ From Eq. (10), it is obvious that $\overline{\text{ind}} = 0$ corresponds to the minimum value of the indicator ind and $\overline{\text{ind}} = 1$ to the maximum value. The normalized indicators $\overline{D_1}$, $\overline{D_2}$, \overline{LG} for each simulation are plotted in Fig. 5.

As expected, the lowest lumen gain is obtained for the case of balloon angioplasty, where no scaffold is present to keep the elastic artery open ($LG = 18\%$ due to the tears which weaken the structure). Obviously, for this case $D_1 = 0$ since no stent is present. The maximum values for LG are acquired when the control stent S_1 ($LG = 48\%$) and the stent with the fewer struts S_3 ($LG = 47\%$) are used. These two stent designs also lead to the highest values for the indicator D_2 , which characterizes (arterial) stress changes.

Generally, Fig. 5 reveals a strong correlation between the indicators LG and D_2 . In other words, the induced stresses in the arterial tissues highly depend on the final dilated state of the artery. Among the three stents, the thinner and more compliant stent S_2 results to the lowest values for all three indicators ($LG = 42\%$). A comparison between the stents S_1 and S_2 indicates that by reducing the thickness of the struts by

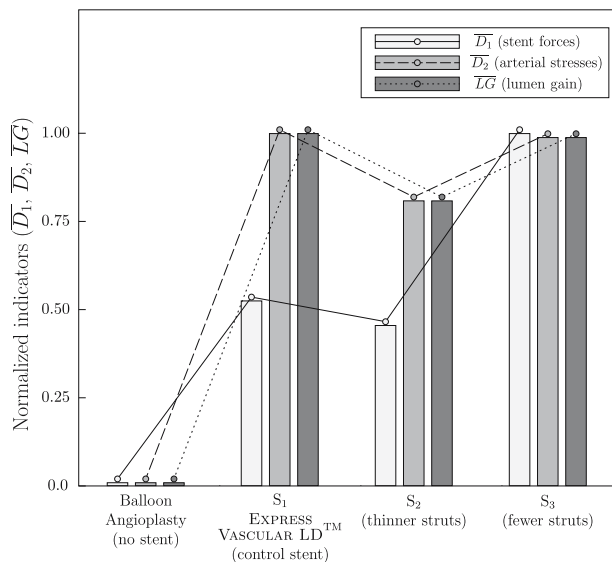


FIGURE 5. Normalized values of the indicators $\overline{D_1}$, $\overline{D_2}$, \overline{LG} obtained from the performed simulations. The indicators characterize the stent contact forces, the induced arterial stresses and the gain of lumen area, respectively.

40%, the achieved lumen gain (\overline{LG}), the contact forces ($\overline{D_1}$), and the (arterial) stress changes ($\overline{D_2}$) reduce by approximately 25%. Remarkably, as can be seen in Fig. 5, stent S_3 shows the highest $\overline{D_1}$ value, hence it generates the highest contact forces on the intimal surface, while at the same time, exhibits comparable values for the indicators $\overline{D_2}$ and \overline{LG} (1% difference) to the control stent S_1 , as previously mentioned. This arises from the geometric characteristics of stent S_3 , since a stent with fewer struts on its periphery is structurally stiffer than a stent with more struts and the same thickness. In the case of S_3 a bigger prolapse value is also expected due to the larger distance between the struts.

It is clear that the above indicators stand for competing interests. An optimal treatment or stent design should, from a clinical point of view, lead to sufficiently enlarged lumen area (large \overline{LG} values). At the same time, it should not induce unnecessary arterial trauma, or in other words, should minimize the changes in stresses of the arterial wall and should not apply high contact forces on the intimal surface (small $\overline{D_1}$ and $\overline{D_2}$ values). The importance of each indicator for an optimization procedure depends on the specific patient and the related patient history.

The results of the simulations performed in this work suggest that the control stent S_1 leads to the most promising results in terms of lumen gain. The same \overline{LG} can also be accomplished by the use of stent S_3 . However, S_3 results in more significant changes in the mechanical environment of the arterial wall expressed through $\overline{D_1}$. Consequently, S_3 produces more local

damage of the intimal surface due to contact forces, for the same outcome. In the case where a stent design that minimizes arterial damage is more preferable over a stent that maximizes lumen gain, the thinner and more compliant stent S_2 is the most appropriate device among the other two. Stent S_2 leads to lower values of the indicators $\overline{D_1}$ and $\overline{D_2}$. Accepting that these scalar measures are linked to arterial tissue damage one may assume that stent S_2 is, consequently, less prone to restenosis. This result is comparable with the outcome of clinical studies,^{21,31} which identified that thinner struts elicit less angiographic restenosis than thicker struts.

DISCUSSION AND CONCLUSION

A detailed computational model of the arterial wall, the medical devices and their contact interaction is of pressing need and of utmost importance for a deeper understanding of the vessel response under supra-physiological loading as occurring during and after stent placement. The availability of a comprehensive model is also important for the optimization of stent structures, and, therefore, of the interventional procedure which often fails due to biological reactions such as restenosis.

In the present work a methodology was proposed that identifies ‘optimal’ stent devices. In particular, we presented a numerical framework able to identify the changes in the mechanical environment of atherosclerotic human lesions that occur due to the interaction with vascular stents. We started by discussing the different important modeling aspects of balloon angioplasty with stenting. We analyzed a stenotic iliac artery and modeled it as a solid continuum composed of four types of tissues (adventitia, media, intima, lipid pool). Despite taking into consideration the inhomogeneity of atherosclerotic lesions, several of the identified arterial tissues with different mechanical properties were combined. In a refined attempt the atherosclerotic patient-specific lesion should be analyzed by using more tissue types. The nonlinear elastic response of each tissue was described by a neo-Hookean material relating to the non-collageneous matrix, in addition to an anisotropic free-energy function, which described the response of the collagen fibers.¹² The different sets of material and structural parameters for each tissue were identified by means of *in vitro* uniaxial tensile tests.¹⁷ Residual stresses were not incorporated into the model due to the lack of experimental data on atherosclerotic human iliac arteries. In order to account for the important inelastic effects of the artery at finite deformations such as plaque fissuring and dissipation, two initial tears were introduced into its load-free configuration at locations prone to crack

initiation. In addition, the nonlinear, anisotropic mechanical response of the balloon catheter was described by a cylindrically orthotropic model, originally introduced by Kioussis *et al.*²² From an industrial partner, the EXPRESS VASCULAR LD™ iliac stent was acquired and a software tool was developed that allowed the generation of the computer model based on a number of geometric parameters. By application of the same parametrization tool, two more stent designs were obtained, one with thinner struts and one with fewer struts.

The interaction between the medical devices (balloon and stent) and the inner arterial wall was solved as a 3D contact problem. To this end, the robust contact approach documented in Kioussis *et al.*²² was adopted. Each target surface was described by means of C^2 -continuous uniform cubic B-spline surfaces, thus avoiding jumps of the normal vectors that would occur during sliding of contacting nodes over linear facet-based discretized surfaces. The nonlinearities arising from the contact interactions and the selected material models lead to computationally expensive simulations. Therefore, in this study only a 3D section of the arterial wall and a stent cell were considered. In order to keep the computational costs as low as possible the smallest cell length ($l_a = 1.4$ mm) was used.

One simulation of balloon angioplasty without stent and three simulations of stenting with the aforementioned different stent designs were performed. All computations showed that the incorporation of the tears at the intima led to a different (principal Cauchy) stress environment in the stenosis. In particular, in that case, the mechanical load was carried by the intima, the non-diseased media, and the adventitia. However, the highest stresses were reported at the vicinity of the tears, hence the induced trauma due to stenting remained localized at the dissection site rather than spreading over the lesion, which is in accordance with the recent study.⁸ It should be noted that the used boundary conditions of the two planar arterial faces affect the stresses in the axial direction. However, after artery dilation the axial stresses are considerably smaller than the circumferential or radial ones, and, therefore, do not particularly influence the study's conclusions. In addition, the artery pressure load during and after stenting was not taken into account since the stresses induced by the stent struts are considered to be much higher than those due to blood pressure. However, in order to study the mechanics of the artery after angioplasty more carefully a refined model should consider the blood pressure.

Next, scalar indicators were defined that allow a judgment on the performance of the used stents and of their interactions with the specific atherosclerotic lesion. These indicators (D_1 , D_2 , LG) are measures of the

contact forces applied from the stent to the intimal surface, of the changes of the mechanical stresses in the individual tissues and of the achieved lumen gain. The results revealed a strong correlation between the lumen gain and the induced stress level. Among the different stent configurations, S_1 and S_3 showed comparable values of the indicators D_2 and LG . Nevertheless, the stent S_3 led to higher values of the contact forces (D_1), being thus possibly a less favorable option for clinicians than the control stent S_1 . Finally, the described method indicated that a choice for the most appropriate stent strongly depends on the optimization criterion. In the case that less vascular trauma was regarded as more important than higher lumen area, the performed simulations suggested stent S_2 with the thinner struts as the optimal stent for the lesion under investigation.

Refinements on the geometric and constitutive models have to be considered in future studies. In particular, a larger-scale model should be studied, considering a representative unit length ($a + b + c$) of the stent (see Fig. 2) or the stent as a whole, and the complete 3D morphology of the artery. A computational analysis on such a basis would lead to local stress concentrations in the non-diseased intima at the stent edges,¹⁷ depending on the lesion-morphology and the utilized stent type. In addition, there is plenty of room for introducing other scalar indicators, which characterize the mechanical field of the arterial wall, for example, stress and damage-based indicators. Apart from the mentioned limitations, the proposed physical and numerical models have the ability to provide clear markers for the patient-specific choice of the optimal stent configuration and should be considered as a further step towards computer aided stenting.

ACKNOWLEDGMENTS

The authors are indebted to Martin Auer and Alexander Wulff for their involvements in providing the geometrical models of the artery and the stent, respectively. The support from BOSTON SCIENTIFIC SVERIGE AB providing the EXPRESS VASCULAR LD™ (Boston Scientific) stents is also acknowledged.

REFERENCES

- ¹Abè, H., K. Hayashi and M. Sato (Eds). Data Book on Mechanical Properties of Living Cells, Tissues, and Organs. New York: Springer-Verlag, 1996.
- ²Auer, M., R. Stollberger, P. Regitnig, F. Ebner, and G. A. Holzapfel. 3-D reconstruction of tissue components for

- atherosclerotic human arteries based on high-resolution MRI. *IEEE Trans. Med. Imaging* 25:345–357, 2006.
- ³Bedoya, J., C. A. Meyer, L. H. Timmins, M. R. Moreno, and J. E. Moore. Effects of stent design parameters on normal artery wall mechanics. *J. Biomech. Eng.* 128:757–765, 2006.
- ⁴Burton, H. M., and W. L. Hunter. Drug-eluting stents: A multidisciplinary success story. *Adv. Drug Deliv. Rev.* 58:350–357, 2006.
- ⁵Castaneda-Zuniga, W. R., A. Formanek, M. Tadavarthy, Z. Vlodaver, J. E. Edwards, C. Zollikofer, and K. Amplatz. The mechanism of balloon angioplasty. *Radiology* 135:565–571, 1980.
- ⁶Fattori, R., and T. Piva. Drug-eluting stents in vascular intervention. *Lancet* 361:247–249, 2003.
- ⁷Gasser, T. C., and G. A. Holzapfel. Physical and numerical modeling of dissection propagation in arteries caused by balloon angioplasty. In: Proceedings of the 3rd IASTED International Conference on Biomechanics, edited by M. H. Hamza. Anaheim: ACTA Press, 2005, pp. 229–233.
- ⁸Gasser, T. C., and G. A. Holzapfel. Modeling plaque fissuring and dissection during balloon angioplasty intervention. *Ann. Biomed. Eng.* 35:711–723, 2007.
- ⁹Hoher, M., J. Wohrle, O. C. Grebe, M. Kochs, H. H. Osterhues, V. Hombach, and A. B. Buchwald. A randomized trial of elective stenting after balloon recanalization of chronic total occlusions. *J. Am. Coll. Cardiol.* 34:722–729, 1999.
- ¹⁰Holzapfel, G. A. *Nonlinear Solid Mechanics. A Continuum Approach for Engineering.* Chichester: John Wiley & Sons, 2000.
- ¹¹Holzapfel, G. A. Determination of material models for arterial walls from uniaxial extension tests and histological structure. *J. Theor. Biol.* 238:290–302, 2006.
- ¹²Holzapfel, G. A., T. C. Gasser, and R. W. Ogden. A new constitutive framework for arterial wall mechanics and a comparative study of material models. *J. Elasticity* 61:1–48, 2000.
- ¹³Holzapfel, G. A., C. A. J. Schulze-Bauer, and M. Stadler. Mechanics of angioplasty: Wall, balloon and stent. In: *Mechanics in Biology*, edited by J. Casey and G. Bao. New York: The American Society of Mechanical Engineers (ASME) AMD-Vol 242/BED-Vol 46, 2000, pp. 141–156.
- ¹⁴Holzapfel, G. A., G. Sommer, C. T. Gasser, and P. Regitnig. Determination of the layer-specific mechanical properties of human coronary arteries with non-atherosclerotic intimal thickening, and related constitutive modelling. *Am. J. Physiol. Heart Circ. Physiol.* 289:H2048–2058, 2005.
- ¹⁵Holzapfel, G. A., G. Sommer, and P. Regitnig. Anisotropic mechanical properties of tissue components in human atherosclerotic plaques. *J. Biomech. Eng.* 126:657–665, 2004.
- ¹⁶Holzapfel, G. A., M. Stadler, and T. C. Gasser. Changes in the mechanical environment of stenotic arteries during interaction with stents: Computational assessment of parametric stent design. *J. Biomech. Eng.* 127:166–180, 2005.
- ¹⁷Holzapfel, G. A., M. Stadler, and C. A. J. Schulze-Bauer. A layer-specific three-dimensional model for the simulation of balloon angioplasty using magnetic resonance imaging and mechanical testing. *Ann. Biomed. Eng.* 30:753–767, 2002.
- ¹⁸Humphrey, J. D. *Cardiovascular Solid Mechanics. Cells, Tissues, and Organs.* New York: Springer-Verlag, 2002.
- ¹⁹Ibrahimbegovic, A., and M. Al Mikdad. Finite rotations in dynamics of beams and implicit time-stepping schemes. *Int. J. Numer. Meth. Eng.* 66:781–814, 1998.
- ²⁰Jang, I.-K., G. Tearney, and B. Bouma. Visualization of tissue prolapse between coronary stent struts by optical coherence tomography. Comparison with intravascular ultrasound. *Circulation* 104:2754, 2001.
- ²¹Kastrati, A., J. Mehilli, J. Dirschinger, F. Dotzer, H. Schühlen, F.-J. Neumann, M. Fleckenstein, C. Pfafferott, M. Seyfarth, and A. Schömig. Intracoronary stenting and angiographic results: strut thickness effect on restenosis outcome (ISAR-STEREO) trial. *Circulation* 103:2816–2821, 2001.
- ²²Kiousis, D. E., T. C. Gasser, and G. A. Holzapfel. Smooth contact strategies with emphasis on the modeling of balloon angioplasty with stenting. submitted.
- ²³König, A., T. M. Schiele, J. Rieber, K. Theisen, H. Mudra, and V. Klauss. Influence of stent design and deployment technique on neointima formation and vascular remodeling. *Z. Kardiol.* 91:98–102, 2002.
- ²⁴Korelc, J. Automatic generation of finite-element code by simultaneous optimization of expressions. *Theor. Comput. Sci.* 187:231–248, 1997.
- ²⁵Lally, C., F. Dolan, and P. J. Prendergast. Cardiovascular stent design and vessel stresses: A finite element analysis. *J. Biomech.* 38:1574–1581, 2005.
- ²⁶Laursen, T. A. *Computational Contact and Impact Mechanics.* Berlin: Springer-Verlag, 2002.
- ²⁷Lee, R. T., H. M. Loree, G. C. Cheng, E. H. Lieberman, N. Jaramillo, and F. J. Schoen. Computational structural analysis based on intravascular ultrasound imaging before in vitro angioplasty: Prediction of plaque fracture locations. *J. Am. Coll. Cardiol.* 21:777–782, 1993.
- ²⁸Liang, D. K., D. Z. Yang, M. Qi, and W. Q. Wang. Finite element analysis of the implementation of a balloon expandable stent in a stenosed artery. *Int. J. Cardiol.* 104:314–318, 2005.
- ²⁹Lyon, R. T., C. K. Zarins, C. T. Lu, C. F. Yang, and S. Glagov. Vessel, plaque and lumen morphology after transluminal balloon angioplasty. Quantitative study in distended human arteries. *Arteriosclerosis* 7:306–314, 1987.
- ³⁰Migliavacca, F., L. Petrini, P. Massarotti, S. Schievano, F. Auricchio, and G. Dubini. Stainless and shape memory alloy coronary stents: A computational study on the interaction with the vascular wall. *Biomech. Model. Mechanobiol.* 2:205–217, 2004.
- ³¹Pache, J., A. Kastrati, J. Mehilli, H. Schühlen, F. Dotzer, J. Hausleiter, M. Fleckenstein, F. J. Neumann, U. Sattelberger, C. Schmitt, M. Muller, J. Dirschinger, and A. Schömig. Intracoronary stenting and angiographic results: Strut thickness effect on restenosis outcome (ISAR-STEREO-2) trial. *J. Am. Coll. Cardiol.* 41:1283–1288, 2003.
- ³²Piegel, L. A., and W. Tiller. *The NURBS Book.* 2nd ed. New York: Springer-Verlag, 1997.
- ³³Schulze-Bauer, C. A. J., C. Mörth, and G. A. Holzapfel. Passive biaxial mechanical response of aged human iliac arteries. *J. Biomech. Eng.* 125:395–406, 2003.
- ³⁴Schulze-Bauer, C. A. J., P. Regitnig, and G. A. Holzapfel. Mechanics of the human femoral adventitia including high-pressure response. *Am. J. Physiol. Heart Circ. Physiol.* 282:H2427–H2440, 2002.
- ³⁵Schwartz, R. S., and T. D. Henry. Pathophysiology of coronary artery restenosis. *Rev. Cardiovasc. Med.* 3(Suppl. 5):S4–S9, 2002.

- ³⁶Serruys, P. W., P. de Jaegere, F. Kiemeneij, C. Macaya, W. Rutsch, G. Heyndrickx, H. Emanuelsson, J. Marco, V. Legrand, P. Materne, J. Belardi, U. Sijwart, A. Colombo, J. Goy, P. van den Heuvel, J. Delcan, and M. Morel. A comparison of balloon-expandable-stent implantation with balloon angioplasty in patients with coronary artery disease Benestent Study Group. *N. Engl. J. Med.* 331:489–495, 1994.
- ³⁷Stary, H. C. *An Atlas of Atherosclerosis Progression and Regression*. New York: Parthenon, 1999.
- ³⁸Stolpmann, J., H. Brauer, H.-J. Stracke, R. Erbel, and A. Fischer. Practicability and limitations of finite element simulation of the dilation behaviour of coronary stents. *Mat.-wiss. u. Werkstofftechn.* 34:736–745, 2003.
- ³⁹Taber, L. A. Biomechanics of growth, remodelling, and morphogenesis. *Appl. Mech. Rev.* 48:487–543, 1995.
- ⁴⁰Taylor, R. L. *FEAP – A Finite Element Analysis Program, Version 7.5 User Manual*. Berkeley, California: University of California at Berkeley, 2005.
- ⁴¹CUBIT Team. *CUBIT 10.0 User's Manual*. Albuquerque, New Mexico, USA: Sandia National Laboratories, 2005.
- ⁴²Wang, D. L., B. S. Wung, Y. J. Shyy, C. F. Lin, Y. J. Chao, S. Usami, and S. Chien. Mechanical strain induces monocyte chemotactic protein-1 gene expression in endothelial cells. Effects of mechanical strain on monocyte adhesion to endothelial cells. *Circ. Res.* 77:294–302, 1995.
- ⁴³Weizsäcker, H. W., and J. G. Pinto. Isotropy and anisotropy of the arterial wall. *J. Biomech.* 21:477–487, 1988.
- ⁴⁴Wentzel, J. J., J. Kloet, I. Andhyiswara, J. A. Oomen, J. C. Schuurbiers, B. J. de Semet, M. J. Post, D. de Kleijn, G. Paterkamp, C. Borst, C. J. Slager, and R. Krams. Shear-stress and wall-stress regulation of vascular remodeling after balloon angioplasty: Effect of matrix metalloproteinase inhibition. *Circulation* 104:91–96, 2001.
- ⁴⁵Wolfram Research Inc. *Mathematica 5.2*. Champaign, Illinois: Wolfram Research, Inc., 2005.
- ⁴⁶Wriggers, P. *Computational Contact Mechanics*. Chichester: John Wiley & Sons, 2002.
- ⁴⁷Wriggers, P., L. Krstulovic-Opara, and J. Korelc. Smooth C^1 -interpolations for two-dimensional frictional contact problems. *Int. J. Numer. Meth. Eng.* 51:1469–1495, 2001.
- ⁴⁸Zhou, J., and Y. C. Fung. The degree of nonlinearity and anisotropy of blood vessel elasticity. *Proc. Natl. Acad. Sci. USA* 94:14255–14260, 1997.